

# Spectral, Electrical, Mechanical, Linear And Nonlinear Optical Studies of 2-Amino-5-Methyl-Pyridinium Phosphate Single Crystals

A. Mohamed Ibrahim<sup>1</sup>, S. Arunachalam<sup>2</sup>

<sup>1,2</sup>Dept of Chemistry

<sup>1</sup>Hindusthan College of Engineering and Technology, Coimbatore – 641 032, Tamil Nadu, India

<sup>1</sup>Research and Development Centre, Bharathiar University, Coimbatore-641046, Tamil Nadu, India

<sup>2</sup>School of Advanced Sciences, Kalasalingam Academy of Research and Education, Krishnankoil-626126, Tamilnadu, India

**Abstract-** The single crystals of 2-Amino-5-methyl-pyridinium phosphate (AMPP) have been synthesised and grown by slow evaporation technique. The grown crystal was characterised by X-ray diffraction analysis. The different vibrational modes of the compound were studied by Fourier transform infrared (FT-IR) spectroscopic analysis. The decreasing tendency of dielectric constant with increasing frequency was shown in dielectric study. The stiffness constant and yield strength were calculated. The Photoluminescence study was also carried out on grown crystal. The Z-scan technique was used to determine the third order nonlinear optical parameters refractive index ( $n_2$ ), absorption coefficient ( $\beta$ ) and susceptibility ( $\chi(3)$ ). The dipole moment, linear polarisability and first order hyperpolarisability values were also calculated.

## I. INTRODUCTION

In the industrial world of today there is a high demand for the charge transferred complexes crystal species. The requirement for better and well characterized charge transferred complex crystals has been the driving force behind the extensive research and development in the optical, magnetic, electrical and biological fields. The CT complexes are formed between an electron rich donor molecule with low ionization potential and an electron deficient acceptor molecule with high ionization potential [1]. CT complexes act as intermediate in wide variety of reactions involving electron rich and electron deficient molecules [2]. Most of the molecules show large nonlinear optical response, with the electron-donor and electron-acceptor groups located at the extreme of a system [3]. It has been recognized that the two-photon optical properties of materials should be affected by the donor-acceptor strength, the molecular structure, the conjugation length and the intermolecular charge transfer [4-6]. The conjugation  $\pi$ -electron moiety provides a pathway for the entire length of conjugation under the perturbation of an external electric field. Fictionalization of both ends of the  $\pi$  bond systems with appropriate electron donor and acceptor group can increase the asymmetric electronic distribution in

either or both the ground and excited states, thus leading to an increased optical nonlinearity [7, 8]. In particular, the strong delocalization of  $\pi$  electrons in the organic backbone determines a high molecular polarizability and thus resulting third order optical nonlinearity [9].

The third order nonlinearity, namely the third order susceptibility of matter has been responsible for different physical phenomena including but not limited to third-harmonic generation, two-photon absorption, nonlinear refraction, four-wave mixing, Raman Spectroscopy, etc., [10]. This research work is only focused on nonlinear refraction. The single crystals of 2-Amino-5-methyl-pyridinium phosphate (AMPP) were grown by slow evaporation solution growth technique in room temperature. The grown crystals were subjected for the various characterization such as Single X-ray diffraction analysis, UV-vis spectroscopy, FTIR, dielectric study, and hardness studies. The third order nonlinear optical parameters like refractive index, absorption coefficient and susceptibility were calculated for the grown crystals.

## II. EXPERIMENTAL

### Synthesis

For the preparation of Single crystals of 2-Amino-5-methyl-pyridinium phosphate (AMPP), the equimolar mixture of 2-Amino-5-methyl-pyridine and phosphoric acid in ethanol was stirred for 2 hours. The solution was then filtered through a quantitative whatmann 41 grade filter paper to remove the suspended impurities. The beaker containing the filtrate was covered using thin polythene sheet to prevent the evaporation quickly. The perforations were made to regulate the evaporation. The beaker was kept aside unperturbed in an atmosphere most suitable for the growth of single crystals. The crystals of title compound was harvested by slow evaporation technique at room temperature. Photograph of grown single crystals has been depicted in Figure 1.



Figure 1. Solution grown crystals of AMPP.

#### IV. RESULT AND DISCUSSION

##### Single crystal X-ray diffraction analysis

The unit cell parameters and the crystal structure for the synthesised compound were obtained on a Bruker AXS Kappa APEX II CCD diffractometer using graphite monochromated MoK $\alpha$  radiation ( $\lambda = 0.71073 \text{ \AA}$ ) at 298 K. The synthesized crystal crystallized in monoclinic system, space group P2<sub>1</sub>/c with unit cell parameters  $a = 10.872 \text{ \AA}$ ,  $b = 9.858 \text{ \AA}$ ,  $c = 11.353(11) \text{ \AA}$ ,  $\alpha = 90^\circ$ ,  $\beta = 108.415^\circ$ ,  $\gamma = 90^\circ$ . The unit cell volume is  $923.18 \text{ \AA}^3$ . The XRD results are in good agreement with the reported values and thus confirm the grown crystal [11]. In the crystalline lattice the synthesized crystal crystallized as protonated 2-Amino-5-methyl-pyridine and deprotonated phosphoric acid. The structure of the compound is stabilized by hydrogen bonding interactions N-H...O, C-H...O, O-H...O.

##### FT-IR Analysis

The FT-IR spectrum of AMPP single crystal was recorded employing Perkin-Elmer FT-IR spectrometer using the KBr pellet technique. The spectrum depicted in the figure 2 shows the presence of characteristic absorption bands due to the varied force constants in the donor and the acceptor species on account of the prevalent charge transfer mechanism. Normally in an acid base reaction, a proton transfer from the acceptor (acid) to the donor (base) is expected to occur. The band at  $3614 \text{ cm}^{-1}$  is due to the N-H stretching vibration. A peak at  $3364 \text{ cm}^{-1}$  is observed due to NH<sub>2</sub> vibration. The O-H stretching vibration is observed at  $3139 \text{ cm}^{-1}$ . The absorptions at 2593 and  $2401 \text{ cm}^{-1}$  are due to O-H stretching vibration of phosphate. The C-N stretching vibrations are observed at 2091 and  $2009 \text{ cm}^{-1}$ . The absorptions at  $1617 \text{ cm}^{-1}$  is due to pyridine ring vibration. The absorptions at  $1398 \text{ cm}^{-1}$  is due to aromatic CH<sub>2</sub> stretching vibration of the aromatic ring. The band at  $1134 \text{ cm}^{-1}$  is due to

P-O stretching vibration. Aromatic NH<sub>2</sub> out-plane bending vibration is observed at 824. The sharp absorption band at  $578 \text{ cm}^{-1}$  is attributed to C-H vibration of pyridine ring.

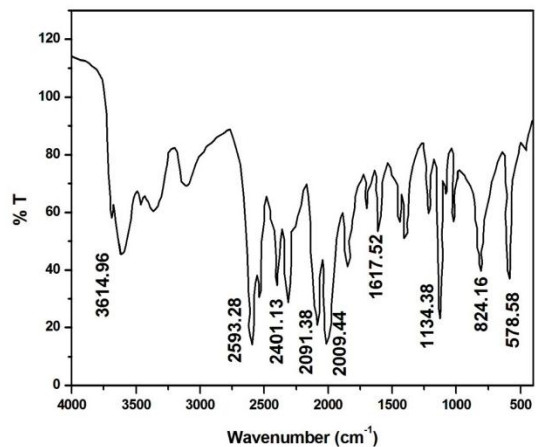


Figure 2 FTIR spectrum of AMPP.

##### UV-Visible Absorption Spectrum

The UV-visible absorption spectrum of AMPP crystal recorded using SYSTRONICS DOUBLE BEAM UV-Vis spectrophotometer in the range 200 – 1200 nm. The UV-Visible spectrum gives limited information about the structure of the molecule because the absorption of UV and visible light involves the promotion of the electron in  $\sigma$  and  $\pi$  orbitals from the ground state to higher energy states. The electronic absorption spectrum of the OS crystal is depicted in figure 3. The spectrum reveals that the strong absorption bands attributed to the charge transfer transition and appears around 319 nm. The longer wavelength absorption band arising due to the promotion of an electron from the highest occupied molecular orbital to the lowest unoccupied molecular orbital confirms the formation of charge transfer molecular complex.

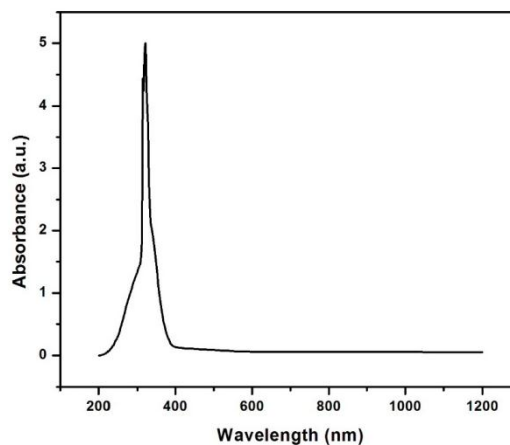


Figure 3 Absorption spectrum of AMPP.

##### UV-Visible Transmission Spectrum

The transmission spectrum plays a vital role in identifying the potential of a NLO material. A given NLO material can be of utility only if it has a wide transparency window. The UV-visible transmission spectrum of grown OS crystals recorded using SYSTRONICS DOUBLE BEAM UV-Vis spectrophotometer in the range 300 – 1200 nm. The spectrum is shown in figure 4. The grown crystal has no absorption beyond the wavelength 330 nm (visible region). Hence this illustrates to know the suitability of the crystal for second harmonic generation and various optical applications [12, 13].

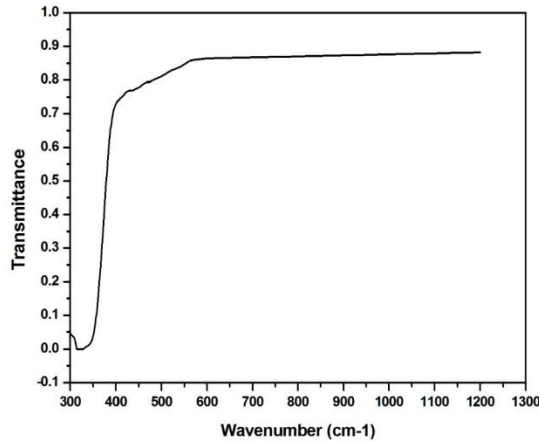


Figure 4 Transmittance spectrum of AMPP.

**Determination of refractive index**

In optoelectronic application it is important to determine the optical behavior of the materials. Knowledge of a material such as optical band gap and extinction coefficient is quite essential to examine the material’s optoelectronic applications [14]. The optical constants are determined from the transmission (T) and reflection (R) spectrum based on the following relations [15].

$$T = \frac{(1 - R)^2 \exp(-\alpha t)}{1 - R^2 \exp(-2\alpha t)}$$

Where t is the thickness and  $\alpha$  is related to extinction coefficient by

$$K = \frac{\alpha \lambda}{4\pi}$$

The reflectance (R) in terms of the absorption coefficient and refractive index (n) can be derived from the relations:

$$R = \frac{1 \pm \sqrt{(1 - \exp(-\alpha t) + \exp(\alpha t))}}{1 + \exp(-\alpha t)}$$

$$n = \frac{-(R + 1) \pm \sqrt{(-3R^2 + 10R - 3)}}{2(R - 1)}$$

The refractive index of the grown crystal was calculated using above relations. Figure 5 shows the energy dependence of refractive index (n) for the grown AMPP crystal. The refractive index increases with increasing energy in lower wavelength region.

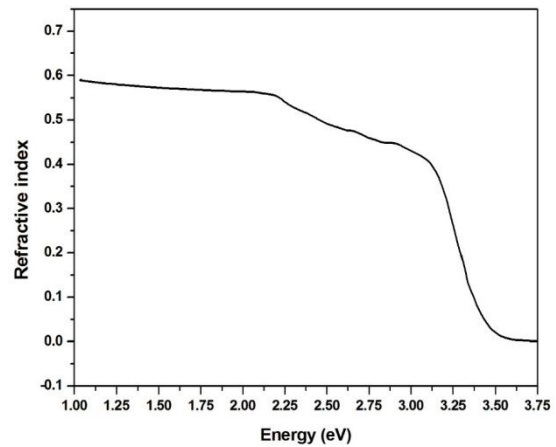


Figure 5 Refractive index Vs Energy of AMPP.

**Dielectric study**

The dielectric study of grown AMPP single crystal was carried. The capacitance of the sample was measured by varying the frequency from 50Hz to 200KHz. Figure 6 shows the plot of dielectric constant ( $\epsilon_r$ ) versus log frequency. The dielectric constant has higher values in the lower frequency region and then it decreases with increasing frequency. The very high values of dielectric constant at low frequencies may be due to the presence of space charge, orientation, electronic, and ionic polarizations. The low value of dielectric constant at higher frequencies may be due to the loss of significance of these polarizations gradually. At high frequency, the defects no longer have enough time to rearrange in response to the applied voltage; hence the capacitance decreases [16]. The variation of dielectric loss with log frequency is shown in Figure 7. The characteristic of low dielectric loss at high frequencies for a given sample suggested that the sample possesses enhanced optical quality with lesser defects and this parameter play a vital role for the fabrication of nonlinear optical devices [17].

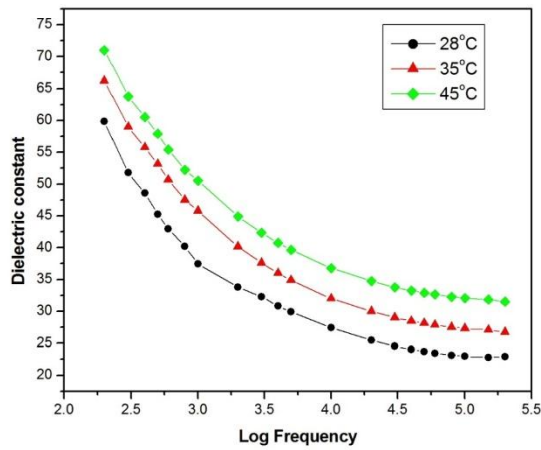


Figure 6 Dielectric constant Vs log f

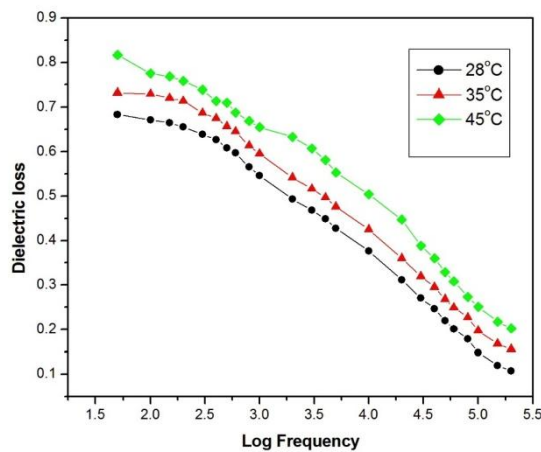


Figure 7 Dielectric Loss Vs log f

**Microhardness study**

Mechanical properties of the grown crystal were studied using a Vickers micro-hardness tester with a Vickers diamond pyramidal indenter attached to an incident light microscope. The static indentations were made at room temperature with a constant indentation time 10 s for all indentations. The indentation marks were made on the surfaces by varying the load from 25 to 300 g. The Vickers microhardness number  $H_v$  of the crystal is calculated using the relation

$$H_v = \frac{1.8544P}{d^2} \text{ kg}/\mu\text{m}^2$$

Where P is the applied load in kg and d corresponds to average diagonal length in micrometre.

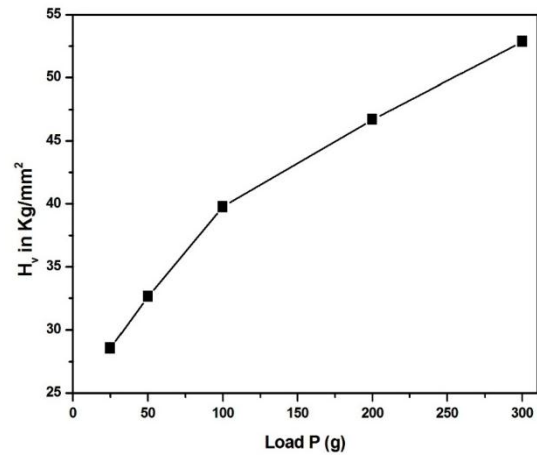


Figure 8 Hardness Vs Load P.

Figure 8 shows the plot between load (P) and  $H_v$  of AMPP single crystal. From the graph, it is very clear that  $H_v$  increases with the increase of load which indicates the reverse indentation size effect. The increase in  $H_v$  with increasing load can be attributed to the electrostatic attraction between the zwitterions present in the molecule. The Meyer's index number was calculated from Meyer's law, which relates the load and indentation diagonal length and is given by

$$P = kd^n$$

$$\log P = \log k + n \log d$$

where k is the material constant and n is Meyer's index.

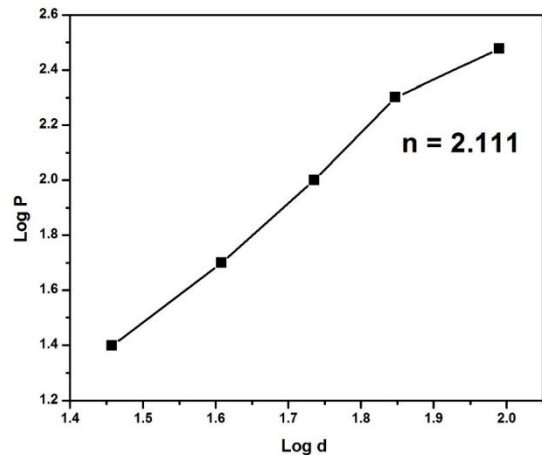


Figure 9 Log P and Log d.

Figure 9 shows the plot between log P and log d. The slope of this straight line plot gives the value of n and is calculated as 2.83.  $H_v$  should increase with increase of P if  $n > 2$  (reverse ISE) and decrease if  $n < 2$  (normal ISE). When  $n = 2$ , the hardness is independent of the load applied and is given by Kick's law [18]. Then value agrees well with the experiment. According to Onitsch [19] and Hanneman [20] n should lie between 1 and 1.6 for harder materials and for

softer materials  $n$  should be above 1.6. Thus APHB belongs to the soft material category ( $n = 2.111$ ). The stiffness constant (C11) gives details about the nature of bonding between the neighbouring atoms. C11 is the property of the material by virtue of which it can absorb maximum energy before fracture occurs. The stiffness constant (C11) is calculated from Wooster's empirical relation [21] given by  $C11 = H_v^{7/4}$ . The variation of stiffness constant (C11) with various loads is shown in Figure 14.

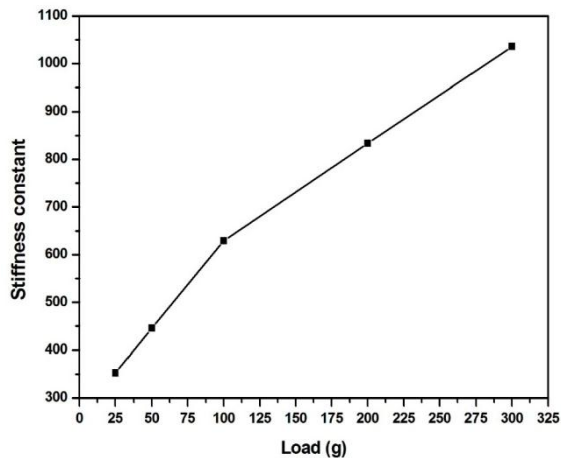


Figure 10. Stiffness constant Vs Load.

From the hardness values, the yield strength ( $\sigma_y$ ) can be calculated. The yield strength is defined as the stress at which the material begins to deform plastically. The value of the yield strength depends on Meyer's index number  $n$ . For  $n > 2$ ,  $\sigma_y$  can be calculated using the expression

$$\sigma_y = \frac{3 - n}{2.9} \left( \frac{12.5(n - 2)}{3 - n} \right)^{n-2} H_v$$

For  $n < 2$ , the yield strength is calculated using the relation

$$\sigma_y = \frac{H_v}{3}$$

It is seen from Figure 10 that the yield strength also increases as load increases.

From the hardness values, the yield strength ( $\sigma_y$ ) can be calculated. The yield strength is defined as the stress at which the material begins to deform plastically. The value of the yield strength depends on Meyer's index number  $n$ . For  $n > 2$ ,  $\sigma_y$  can be calculated using the expression

$$\sigma_y = \frac{3 - n}{2.9} \left( \frac{12.5(n - 2)}{3 - n} \right)^{n-2} H_v$$

It is seen from figure 11 that the yield strength also increases as load increases.

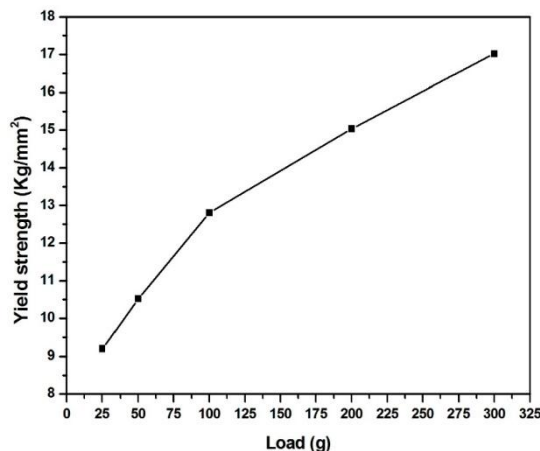


Figure 11. Yield strength Vs Load

### Photoluminescence study

The photoluminescence (PL) studies were carried to evaluate lower concentration of defects and transitional band gaps. The impurity on absorption of light gives rise to bound excited state from which it returns to its ground state abiding in the analysis of colour centre creation mechanism [22]. The PL property of organic complex basically depend on presence of localized  $\pi$ -electron systems in molecules. Nevertheless, the intensity of incident beam and the density of photons also alter the PL signal from a crystalline compound. The figure 12 shows the PL emission spectrum of AMPP crystal. The maximum emission wavelength is observed to be at 407.3 nm. The emission peak at 407.3 nm corresponds to violet wavelength emission. The violet emission is due to the donation of protons to the pyridine group from phosphoric acid in the molecule.

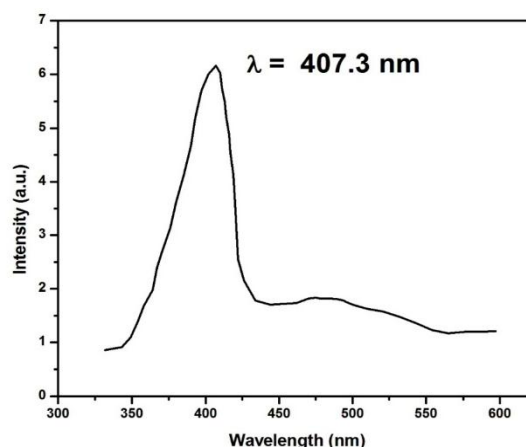
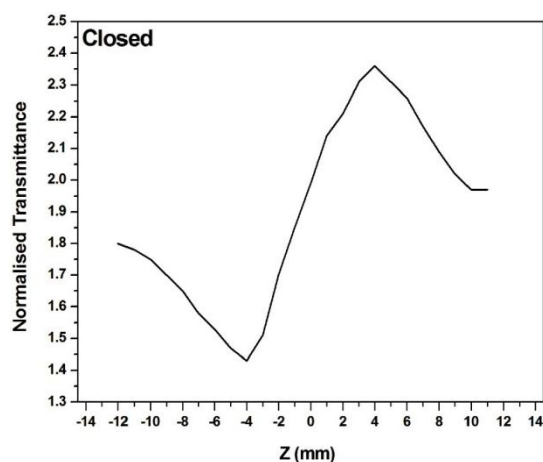


Figure 11 Photoluminescence spectra of AMPP.

### Z-scan study

The Z-scan technique is generally used to measure the magnitude and sign of nonlinear refraction ( $n_2$ ) and nonlinear absorption coefficient ( $\beta$ ), simultaneously [23]. The study of nonlinear refraction by the Z-scan method depends on the position (Z) of the crystal along a focused laser beam. Depending on the positive or negative nonlinear refraction, the sample causes an additional focusing and defocusing of light. The valley followed by a peak in the transmittance curve is the signature for positive nonlinearity and is known as the self-focussing effect. Figure 13 shows the normalized transmittance T with closed aperture as a function of the distance z along the lens axis in the far field. The closed aperture transmittance data confirms the positive nonlinearity of the crystal. This is due to the local variation of refractive index with temperature. Figure 14 shows the open aperture normalized transmittance curve. There will be a maximum transmittance at the focus for saturable absorber samples. Multi-photon absorption reduces the peak transmittance and augments the valley [24]. The minimum transmittance at focus shows the multi-photon absorption effect in the crystal.



**Figure 12.** Normalized transmittance with closed aperture as a function of Z position

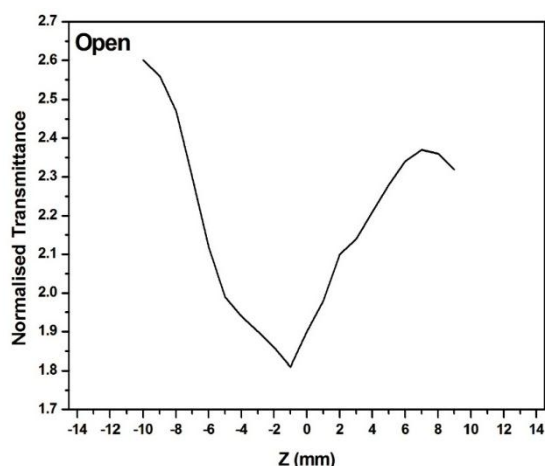


**Figure 13.** Normalized transmittance with open aperture as a function of Z position

From the normalized transmittance curve, the nonlinear refractive index ( $n_2$ ), nonlinear absorption coefficient ( $\beta$ ) and Third order susceptibility  $\chi^{(3)}$  has been calculated [25] for the AMPP crystals. The calculated nonlinear refractive index ( $n_2$ ), nonlinear absorption coefficient and third order susceptibility values of APDP are  $1.02 \times 10^{-9}$  cm/W and  $3.909 \times 10^{-8}$  cm<sup>2</sup>/W and  $2.09 \times 10^{-8}$  esu. The results reveals the positive refractive index, the self-focusing nature and the two-photo absorption process of the crystal.

## V. CONCLUSION

The single crystals of 2-Amino-5-methyl-pyridinium phosphate were synthesized and grown by adopting slow evaporation technique at room temperature. In single crystal confirmed the centrosymmetry space group of the grown crystals. The presence of various functional groups in crystal was analyzed by The FTIR spectrum. UV-vis absorption analysis reveals the electron transition around wavelength 320 nm which confirms the formation of charge transfer in grown crystal. The transparency of the grown crystals was studied through UV-Vis transmission spectra. The crystal showed the transparency beyond 330 nm wavelength (visible) region which is a desire property for various NLO applications. The characteristic of low dielectric loss at high frequencies for grown crystals suggested that the grown crystals possessed enhanced optical quality with lesser defects. The Vickers microhardness test revealed that the grown crystal was a soft material. The photoluminescence studies were carried to evaluate lower concentration of defects and transitional band gaps. The Z-scan results reveals the self-focusing nature of the crystal.

## REFERENCES

- [1] M. Kidwai, S. Saxena, S. Rastogi, R. Venkataramanan, *Curr. Med. Chem. Anti- Infective Agents* 2004, 2, 269.
- [2] F.L. Zhao, B.Z. Xu, Z.Q. Zhang, S.Y. Tong, *J. Pharm. Biomed. Anal.* 1999, 21, 355.
- [3] Dr. J. Thomas Joseph Prakash J. FelicitaVimala M. Lawrence *Int. J. of Comp. Appl.* 2010, 8, 0975.
- [4] H.M. Kim, M.S. Seo, S.-J. Jeon, B.R. Cho, *J. Chem. Commun.* 2009, 47, 7422.
- [5] B.A. Reinhardt, L.L. Brott, S.J. Clarson, A.G. Dillard, J.C. Bhatt, R. Kannan, L.X. Yuan, G.S. He, P.N. Prasad, *J. Chem. Mater.* 1998, 10, 1863.
- [6] D. Beljonne, W. Wenseleers, E. Zojer, Z. Shuai, H. Vogel, S.J.K. Pond, J.W. Perry, S.R. Marder, J.-L. Bredas, *J. Adv. Funct. Mater.* 2002, 12, 631.
- [7] R T. Bailey, G. Bourhill, F R. Cruickshank, D. Pug, J N. Sherwood and G S. Simpson, *J. Appl. Phys.* 1993, 73, 1591.

- [8] W .Yang, L .Yu, T L. Zhang, J G. Zhang, F L. Ren, Y H. Liu, R F. J Y. Wu and Guo, J. Mol. Struct. 2006, 255-260, 794.
- [9] Nalwa, H, S.; Watanabe, T.; Miyata, S. Organic Materials for Second-Order Nonlinear Optics in Nonlinear Optics of Organic Molecules and Polymers, CRC Press, Florida, U.S.A., 1997.
- [10] Boyd, R. W. Nonlinear Optics; Third ed.; Academic Press: Boston, 2008.
- [11] Hai Feng, Cui-Rong Sun, Li Li, Zhi-Min Jin and Bin Tu, Acta Cryst. 2005, E61, 1983.
- [12] S. Anie Roshan, C. Joseph, M.A. Ittyachen, Matter. Lett. 2001, 49, 299.
- [13] V.Venkataramanan, S. Maheswaran, J.N. Sherwood, H.L. Bhat, J. Cryst. Growth 1997, 173, 605.
- [14] M.Dongol, Egypt, J. Solids, 2002, 25, 33.
- [15] B.L. Zhu, C.S. Xie, D.W. Zeng, W.L. Song, A.H. Wang, Mater. Chem. Phys. 2005, 89, 148.
- [16] P.W. Zukowski, S.B. Kantorow, D. Maczka, V.F. Stelmakh, Phys. Stat. Sol. A 1989, 112, 695.
- [17] C. Balarew, R. Duhlew, J. Solid Sate Chem. 1984, 55, 1.
- [18] K.K. Bamzai, P.N. Kotru, B.M. Wanklyn, Appl. Surf. Sci. 1998, 133, 195.
- [19] E.M. Onitsch, Microscopia 1947, 2, 131.
- [20] M. Hanneman, Metall. Manch 1941, 23, 135.
- [21] W.A. Wooster, Rep. Prog. Phys. 1953, 16, 62.
- [22] Shahil Kirupavathy, Stella Mary S, Srinivasan P, Vijayan N, Bhagavannarayana G, Gopalakrishnan R. J. Cryst. Growth 2007, 306, 102.
- [23] M. Sheik-Bahae, A. A. Said, and Van E.W. Stryland, Opt. Lett. 1989, 14, 955.
- [24] M. Sheik-Bahae, A.A. Said, T.H. Wei, D.J. Hagan, E.W. Van Stryland, IEEE J. Quantum Electron. 1990, 26, 760.
- [25] R. Ashok Kumar, R. Ezhil Vizhi, N. Vijayan, G. Bhagavannarayana and D. Rajan Babu, J. Pure Appl. & Ind. Phys. 2010, 1, 61.